applied sciences

MDPI

Article

The Effect of EN Ratio and Current on Microstructural and Mechanical Properties of Weld Joined by AC-GMAW on Square Groove Butt Joints

Adeel Ikram [1] and Hyun Chung *

Department of Mechanical Engineering, KAIST 291, Daehak-ro, Yuseong-gu, Daejeon 34141, Korea; adeelose@kaist.ac.kr

* Correspondence: hyunny92@kaist.edu; Tel.: +82-42-350-1513

Academic Editor: Hai-Lung Tsai

Received: 24 January 2017; Accepted: 3 March 2017; Published: 7 March 2017

Abstract: In the present work, the effect of welding current and electrode negative (EN) ratio on microstructure and mechanical properties of square groove butt joint produced by alternating current gas metal arc welding (AC-GMAW) process has been investigated. The experiments were conducted using different combination of welding current ranging from 150 A to 250 A with three distinct EN ratios i.e., 0%, 30% and 50% on 5 mm thick steel plates at a constant joint gap of 1 mm and welding speed of 10 mm/s. The effect of current and EN ratio on welding soundness was evaluated through optical microscopy, tensile tests and micro-hardness mapping. The results revealed that, at higher values of currents, an increase in EN ratio resulted an increase in penetration depth. It was found that at a current of 250 A and a 50% EN ratio, the deep penetration was obtained. Tensile test results showed that the tensile strength properties improved with increasing current. Furthermore, the micro-hardness distribution was not strikingly affected by changing the EN ratio.

Keywords: AC-GMAW; EN ratio; thick plate; mechanical properties

1. Introduction

Gas metal arc welding (GMAW) is one of the most commonly used welding processes to join a wide range of materials. It is an important constituent for the fabrication of pressure vessels, power plants, ships structures, aero-engine components and steam pipes. The further development of GMAW processes focuses on the possibilities of higher material deposition with the reduced heat input to the base metal (BM) and to raise the weldability of the materials with less heat affected zone (HAZ) and spatters. In recent years, pulsed alternating current gas metal arc welding (AC-GMAW), an advanced variant of conventional GMAW, has emerged, a relatively new welding process owing to its distinct characteristics [1,2]. The pulsed AC-GMAW process contains two distinct portions of the pulse. The electrode positive (EP) portion of the pulse provides better arc stability similar to conventional GMAW process, whereas the electrode negative (EN) portion of the pulse helps in reducing the problems such as burn-through, gap-bridging, and distortion because of low heat input to the BM [2]. Being the low heat input process, heat sensitive materials like ultra-high strength steels (UHSS) would get better mechanical properties in the HAZ [3]. However, the successful application of the AC-GMAW process involves the better understanding of its arc behavior and heat distribution in the weldment. In the case of the conventional direct current gas metal arc welding (DC-GMAW) process, significant efforts have been made to study the process behavior in terms of arc stability and weldment, but very few studies have been reported and found in the technical and scientific literature in the case of the pulsed AC-GMAW process. Moreover, most of the studies on pulsed AC-GMAW have been performed on aluminum welding due to its gap bridging capability as discussed by [4–6].

Park et al. [7] investigated the effect of the EN ratio on the wire melting rate, arc melting phenomenon and drop size in the pulsed AC-GMAW process in aluminum welding. They found that, with the increase in EN ratio, the drop sizes and wire melting rate increased, whereas the heat supplied to the BM decreased. Kumar et al. [8] investigated the microstructure and mechanical properties of butt and overlap welding joints of 1 mm thin 6082 aluminum sheets. They reported that the depth of penetration can be controlled by adjusting the EN ratio. Moreover, shallow penetration was observed with an increase in EN ratio, which resulted in excellent welding of thin sheets. For the application of the AC-GMAW process on steel plate welding, initial efforts were put by Vilarinho et al. [9], who studied the effect of different waveforms and EN ratios on the arc and metal transfer instabilities. They carried out bead on plate (BOP) welding on mild steel using high speed imaging. They observed spatter generation and arc instabilities at high EN ratios. Nascimento et al. [10] performed experiments on steel with high EN ratios. They reported that with the increase in EN ratio, the penetration depth decreased while the reinforcement height increased. Later, Monteiro and Scotti [11] reported that using long EP durations in steel welding, heat was concentrated on the base material, which may have resulted in reasonable penetration depths. However, they found a decrease in penetration depth with an increase in EN duration. Arif and Chung [12] investigated the metal transfer behavior in the AC-GMAW process in order to predict the drop size. An analytical simulation based on force displacement model was used to predict the drop size in AC-GMAW and the results were validated with experiments. A reasonable agreement was found. Kim and Chung [13] analyzed the wire melting phenomenon in the pulsed AC-GMAW process using BOP welding on steel plates. A new form of the wire melting rate equation for the AC-GMAW process is proposed based on energy conservation theory and arc physics. Kiran et al. [14] studied the arc and metal transfer behavior in pulsed DC and AC gas metal arc welding processes using high speed imaging synchronized with current and voltage waveforms at different electrode negative ratios. They proposed regression models to predict the arc root dimensions as a function of the EN ratio, current, voltage and time using BOP welding. They found decrease in peak temperatures in the weldment with an increase in EN ratio. Initially, the AC-GMAW process was applied for thin steel plates welding, but, in the past few years, researchers have observed higher penetration with the improved current waveform as discussed by Arif and Chung [15]. With the introduction of a modified AC-GMAW waveform, reasonable penetration was observed. An improved AC-GMAW process has been developed, which has a peak duration in the electrode negative period. Figure 1 shows the shape of the improved current waveform of AC-GMAW. The pulsating waveform is divided into two regions i.e., EP and EN regions. In the EP region, the parameters such as I_{EP_p}, I_{EP_b}, t_{EP_p} and t_{EP_b} represent the peak current, base current, peak time duration and base time duration, respectively. In the EN region, parameters such as I_{EN_p}, I_{EN_b}, t_{EN_p} and t_{EN_b} represent peak current, base current, peak time duration and base time duration, respectively. Arif and Chung [15] used the improved waveform and conducted BOP welding at different average values of current and EN ratio and presented the results in terms of bead widths and reinforcement height. They reported that deep penetration became prominent at higher welding currents. Further studies are needed to apply this AC-GMAW process with improved waveform for thick plate welding, owing to its benefits of high material deposition rate and arc stability. In the present work, pulsed AC-GMAW process with improved waveform has been applied experimentally on 5 mm thick plate welding in square butt joint configuration with reasonable welding speed. The resultant microstructures and mechanical properties were analyzed.

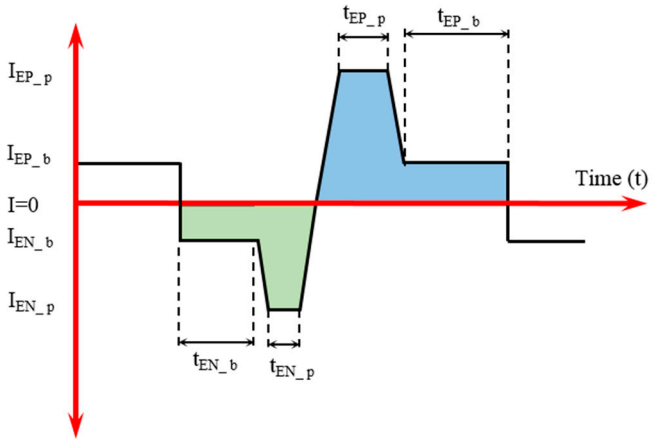

Figure 1. Schematics of the improved current waveform.

2. Experimental Procedure

The commercially available SS400 steel plates with thickness of 5 mm (Dongkuk Steel Mill Co., Ltd., Seoul, Korea) were taken as base material for this study. Table 1 shows the nominal chemical composition of SS400 steel. The butt-weld joints were made from two steel plates having dimensions 250 mm × 125 mm × 5 mm connected via square groove configuration with a fixed joint gap of 1.0 mm. The two steel plates were properly aligned using magnetic clampers and 1 mm joint gap was accurately maintained using steel gauge. For connecting the ends of plates, tack welding was carried out. At one side of the plates, a ceramic backing strip was attached. A steel filler wire ER-70S having a 1.2-mm diameter was used in all experiments. Table 2 lists the chemical composition of ER-70S type welding wire (Forney Industries Inc., Fort Collins, CO, USA).

Table 1. Chemical composition of BM.

C	Si	P	Mn	S	Fe
0.18	0.037	0.016	0.43	0.002	Balance

Table 2. Chemical composition of filler wire (ER-70S).

C	Si	P	Mn	Cr	S	Mo	Ni	Cu	V	Fe
0.06–0.15	0.45–0.75	0.025	1.40–1.85	0.15	0.035	0.15	0.15	0.50	0.03	Balance

The welding tests were carried out by an automatic alternating current gas metal arc welding (AC-GMAW) welder (OTC Daihen Inc., Tipp City, OH, USA). A DW-300 power supply manufactured by OTC Daihen Inc. [16] was used to conduct the welding experiments. The welding torch (OTC Daihen Inc., Tipp City, OH, United States) was kept fixed, and the workpiece was moved at a constant speed of 10 mm/s by using a linear stage system. The welding torch was held perpendicular to the base plate. By using a shielding gas blending system (Chiyoda Seiki Co., Ltd., Kobe, Japan), a controlled amount of shielding gases Ar-20% CO_2 at a flow rate of 18 l/min was provided. The contact tip to workpiece distance (CTWD) was kept at 25 mm with an average electrode extension of 18 mm. Temperature measurements were performed at 20 Hz using K-type thermocouples integrated with the National Instruments (NI) thermocouple card 4353. Figure 2 shows the experimental schematics of the welding process and position of the attached thermocouples in the welding tests.

Due to a large number of variables in the welding process such as current, EN ratio, welding speed, gap between plates, thickness and geometry of the base plate. In the current study, real welding experiments were performed to investigate the effect of current and EN ratio on the joint properties. Average current (Ia) ranges from 150 A–250 A with an increment of 25 A were used during the welding tests, whereas the three distinct EN ratios such 0%, 30% and 50% were selected. The current

pulse corresponding to three EN ratios at average welding current of 200 A has been presented in Figure 3. A total of 15 experimental runs were carried out with each combination of Ia and EN ratio.

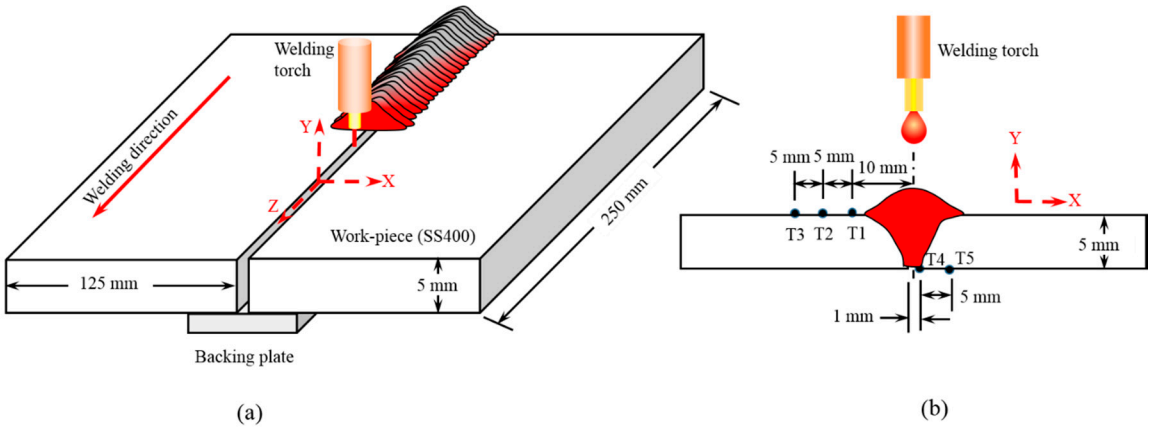

Figure 2. (**a**) Experimental schematics used in the welding tests (**b**) position of thermocouples on base plate.

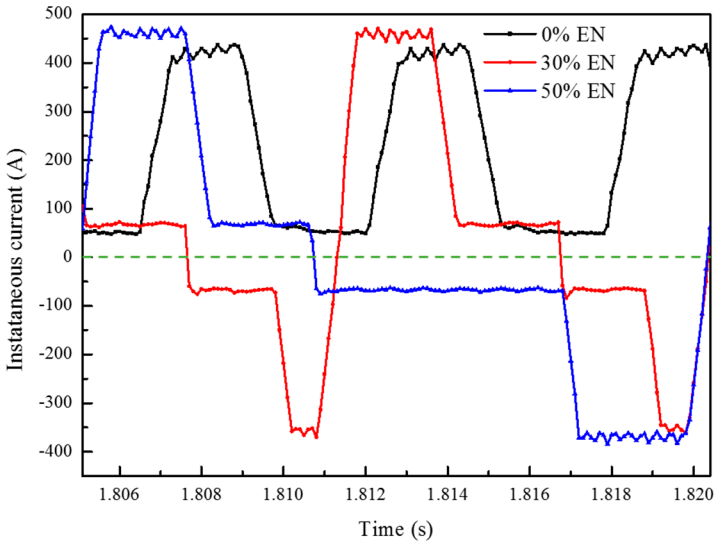

Figure 3. Current pulses at different EN (electrode negative) ratios.

3. Results and Discussion

In the following sections, the thermal behavior, microstructures and mechanical properties of welding tests have been discussed.

3.1. Thermal Behavior

The thermal behavior of the process was analyzed by recording the temperatures at different locations on the base plate. Three thermocouples were positioned on the top side of the plate at distances of 10 mm (T1), 15 mm (T2) and 20 mm (T3) from the weld centerline, whereas two thermocouples were placed at the bottom of the plate (T4), one at the corner of the plate, and the other 5 mm (T5) away from the weld centerline. The schematics of positioning the thermocouples on the top and bottom of the plate is presented in Figure 2. The peak temperatures were measured and graphed against EN ratio at Ia of 175 A in Figure 4. For an EN ratio of 0%, the filler wire acted as an anode and BM acted as a cathode during the complete pulse duration. The resultant temperatures behaved similarly to the usual pattern on DC-pulsed GMAW. However, for an EN ratio of 30% and 50%, the filler wire switched its polarity in each cycle of the pulse. Slightly higher peak temperatures were observed at 30% EN ratio. For an EN ratio of 30%, the filler wires acted as 30% cathode and BM

acted as a 70% anode of the total pulse duration. The cumulative droplet and arc heat generated as a result of ion bombardment in the arc plasma provided a higher amount of heat to the workpiece. Almost 50 °C higher temperatures were recorded at an EN ratio of 30%. For an EN ratio of 50%, the filler wire and BM equally acted as a 50% anode and cathode of the total pulse duration. At a 50% EN ratio, the EP duration was kept the same as in the case of 30%; however, the EN duration was increased to get the 50% EN ratio. The change in the EN duration resulted in the change of heat generation behavior in the arc column. The longer EN duration resulted in the higher temperature gradient away from the weld centerline. As a result of cooling effect on joint sides, low temperatures were recorded at 50% EN. From the above findings, it may be concluded that the heat input in the pulsed AC-GMAW process can be controlled by changing the amount of the electrode negative cycle. Figure 5 shows the recorded temperature with respect to time at Ia of 250 A and 50% EN ratio. A rapid increase in temperature (T4) at the bottom corner of the joint was observed, which is equal to the melting point of the SS400. Deeper penetration was expected due to very high temperatures at the centerline of welding joints.

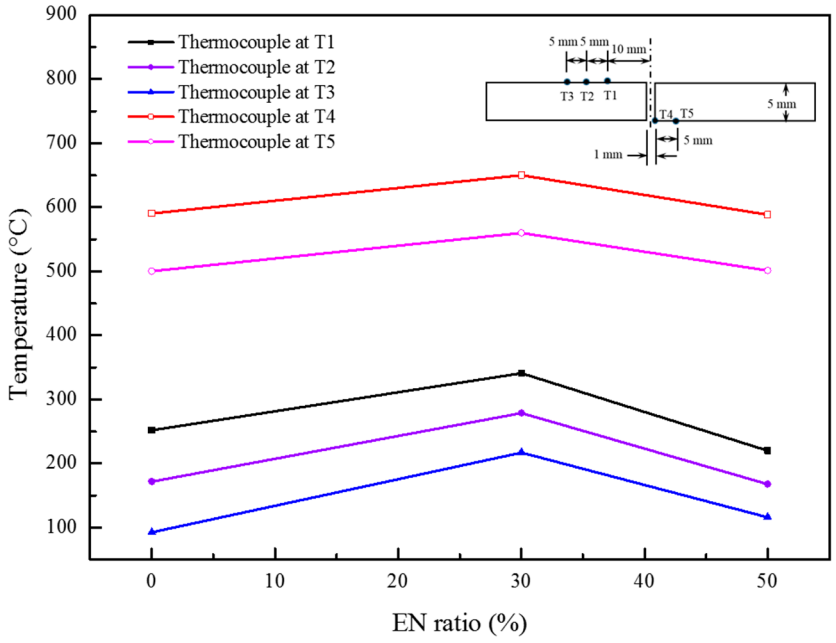

Figure 4. Peak temperatures at current 175 A.

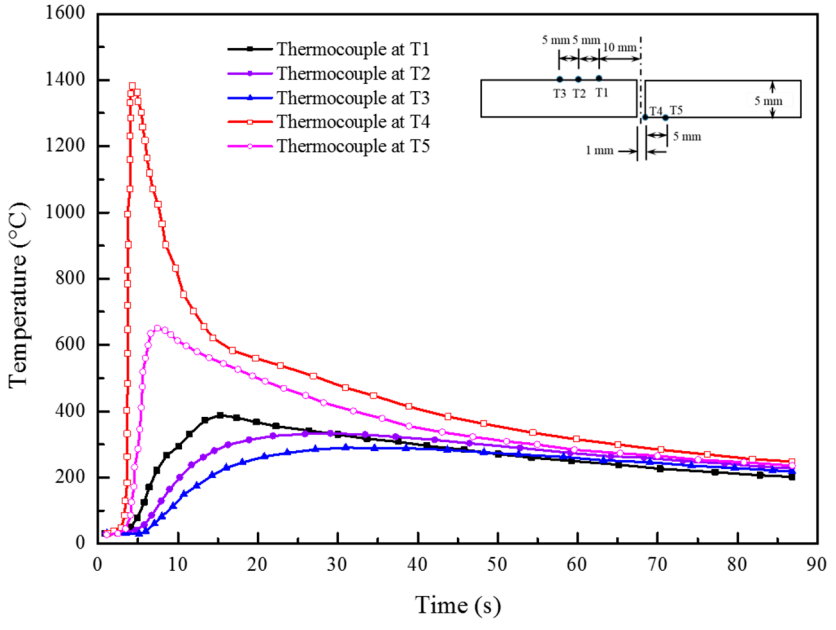

Figure 5. Thermocouple temperatures at current 250 A and 50% EN ratio.

3.2 Macro-Section Analysis and Weld Morphology

To understand the bead shape obtained at different settings of current and EN ratio, macro-sections of welds were analyzed. Figure 6 shows the macro-sections of welds obtained at varying settings of current and EN ratio. The dotted line in macro-section represent fusion boundary (FB).

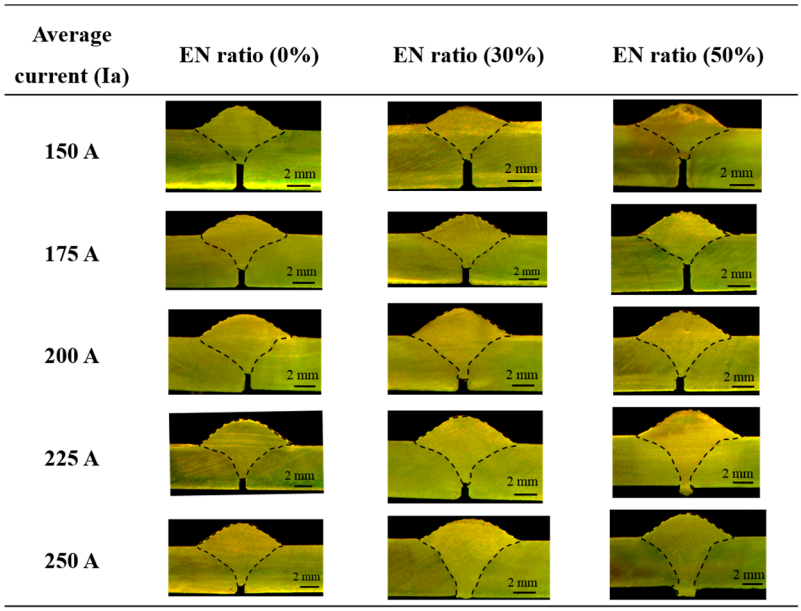

Figure 6. Macro-sections of welded joints at different Ia and EN ratio.

Different bead shape parameters such as penetration depth (*P*), bead width (*W*), reinforcement height (*R*) were measured and the resultant findings were presented in Figures 7–9, respectively. At lower values of currents, the penetration depth decreased with the increased in EN ratio. The penetration depth is less at 50% EN ratio as compared to 0% and 30% at lower value of currents. It is observed that at higher values of currents, the increase in EN ratio resulted in an increase in penetration depth. At Ia of 225 A and 250 A, an increase in EN ratio resulted in an increase in penetration depth. However, it is more noticeable at a 50% EN ratio. The maximum penetration depth was achieved at a 50% EN ratio. The increase in the penetration depth at higher values of currents and EN ratio was a result of the intense plasma jets generated along the weld pool axis. The intense plasma jets generated in the weld pool axis resulted in the higher temperatures at the center, which resulted in finger-like penetration. The above results are in reasonable agreement with earlier results published by Arif and Chung [15] on BOP welding. Increasing the EN ratio at high currents results in deep penetration, which is very useful for thick plate welding.

According to Figure 8, at an EN ratio of 30% and 50%, bead width increased with an increase in current from 150 A to 225 A, and it decreased at a current of 250 A. The reduction of bead width at higher Ia of 250 A is due to the molten metal deep penetration in the weld joint axis. As a result, a low value of bead width was obtained. The maximum bead width was obtained at an Ia of 225 A and a 50% EN ratio. At an EN ratio of 0%, bead width increased with an increase in Ia up to 200 A, and then it decreased with the increase in Ia. Figure 9 shows the comparison of reinforcement height at different EN ratio and Ia. It was found that reinforcement height increased with an increase in Ia from 150 A to 225 A and it decreased at an Ia of 250 A. Maximum reinforcement height was obtained at Ia of 225 A and 0% EN ratio.

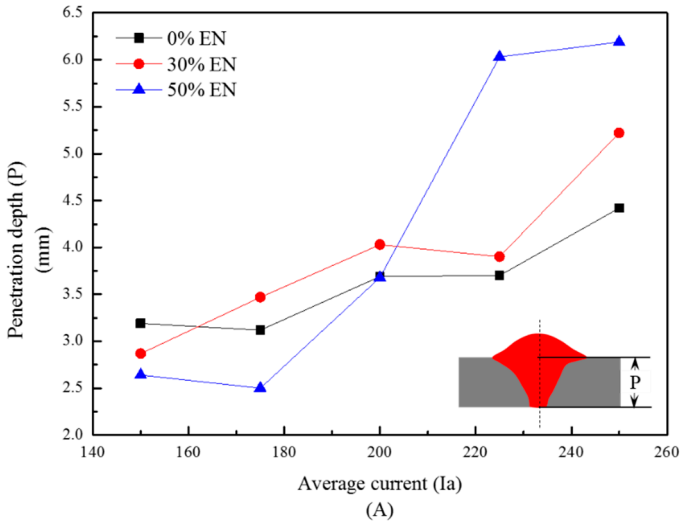

Figure 7. Comparison of penetration depth (*P*) at different EN ratio and Ia.

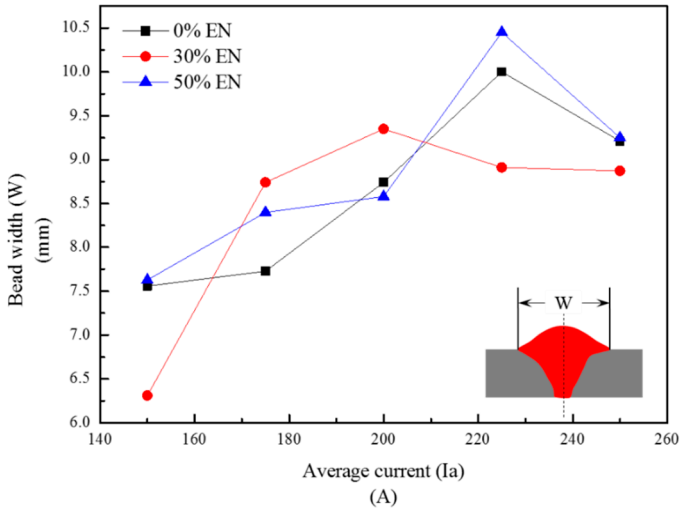

Figure 8. Comparison of bead width (*W*) at different EN ratio and Ia.

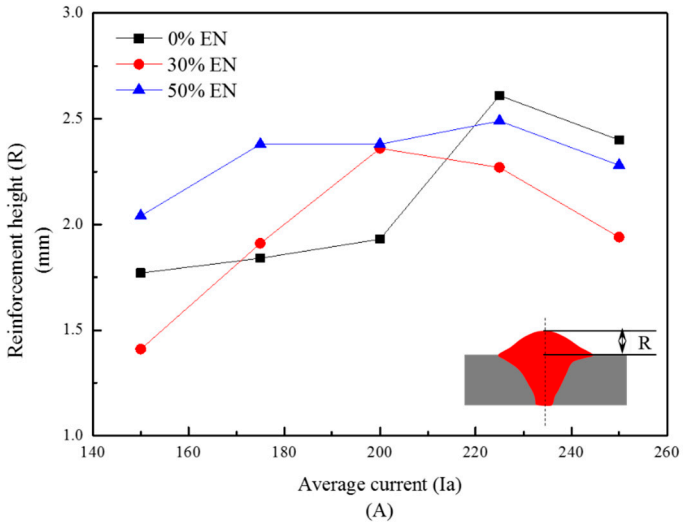

Figure 9. Comparison of reinforcement height (*R*) at different EN ratio and Ia.

The macrographs of welded joints at Ia of 250 A with different EN ratios are presented in Figure 10. The surface appearance of the weld bead revealed spatter free weld joints at all EN ratios.

Weld face showed reasonable weld quality in all cases. However, at Ia of 250 A and a 0% EN ratio, no penetration of molten metal in the root side was observed. However, at a 30% EN ratio, reasonable root side penetration was observed. At a 50% EN ratio, root side showed the desired penetration throughout the weld line. However, it is noticed that the excess of deposited molten metal on the top of the plate requires higher welding speed and optimal joint gap. Macro-section analysis shows that the sound weld joints can be obtained in single pass welding of a 5-mm thick steel plate using higher value of currents and EN ratio. Furthermore, good gap bridging capability is obtained during pulsed AC-GMAW of thick steel plates. Among many factors, joint gap bridging ability of the deposited molten metal is one of the principal factors affected by joint gap tolerance. The appropriate joint gap results in optimal gap filling. With a small joint gap, the deposition of molten filler metal caused a build-up of metal on top of the weld, leaving the weld with excess weld metal profile. As a result, the required joint lacks completely filled grooves. Similarly, with a large joint gap, the deposition of molten metal may cause a lack of metal on the top of the weld. The joint gap has a significant effect on joint sides and deep penetration. Therefore, further detailed study is required to estimate the required joint gap for optimal filling of molten metal with appropriate welding speed at varying thickness of plates.

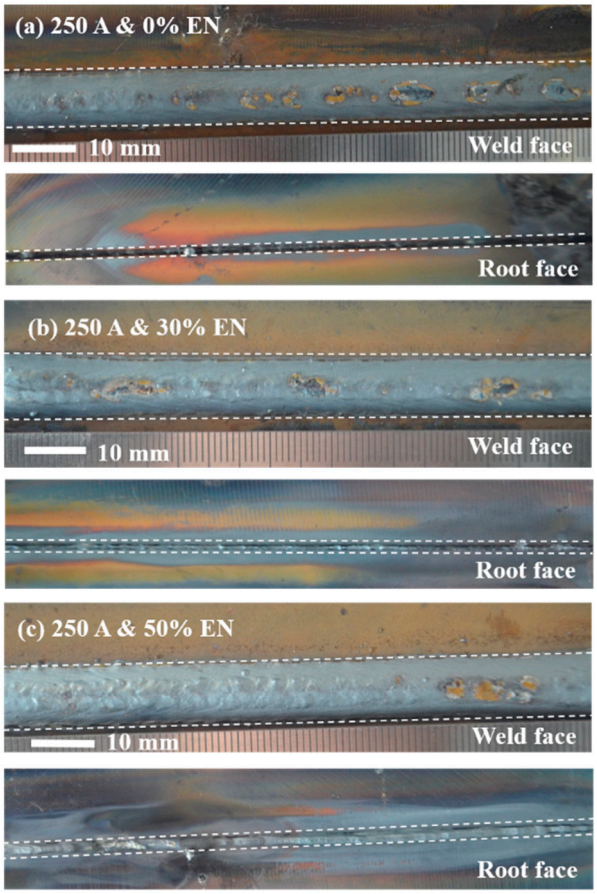

Figure 10. Shows weld macrographs, i.e., weld face and root face at different EN ratio settings (**a**) 250 A, 0% EN; (**b**) 250 A, 30% EN; and (**c**) 250 A, 50% EN.

3.3. Tensile Testing

The tensile strength shows the ability of the workpiece to resist elastic and plastic deformation and fracture under loads. To assess the mechanical properties of the welded joints, the tensile tests were performed by a universal testing machine (UTM) (INSTRON, Norwood, MA, USA). For tensile tests, the required samples were cut from the welded workpieces according to American National Standard (AWS B4.0:2007) specifications. The specimen specifications for tensile test are presented in Figure 11.

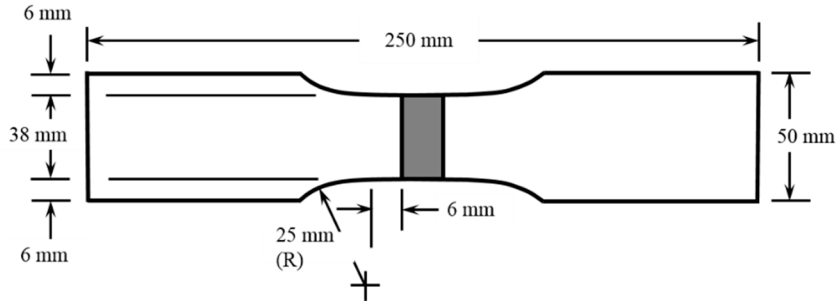

Figure 11. Tensile test specimen dimensions.

The tensile tests for 15 samples were carried out and the resultant mechanical properties of welded joints such as ultimate tensile strength (UTS), yield strength (YS) and percentage elongation (δ) are listed in Table 3. For the calculation of UTS and YS, the area was calculated by multiplying thickness of plate, i.e., 5 mm with the width of the specimen at the weld bead i.e., 38 mm. In terms of welding current, the highest value of UTS was obtained at 250 A, whereas the lowest UTS was observed at 150 A. It is due to the fact that increasing current resulted in more heat input to the BM. As a result, penetration depth increased and proper fusion occurred. Figure 12 shows the stress vs. displacement curve at Ia of 150 A and three distinct EN ratios. It was found that at a current of 150 A, an increase in EN ratio resulted in an increase in UTS and δ. It was noticed that UTS and δ were increased 3.9% and 11.4%, respectively, when EN ratio was increased from 0% to 50%. The fracture locations of the joints have been shown in an inset of Figure 12. It is interesting to note that, irrespective of EN ratio, the fracture for all samples occurred near the FB and away from the weld centerline. It happened because of the incomplete fusion across the joint sides as sufficient heat for melting the joint sides was required. Similarly, for Ia of 175 A as shown in Figure 13, the quite similar behavior was observed. When EN ratio was increased from 0% to 50%, UTS and δ were increased to 1.5% and 8.2%, respectively. Failure of the butt-welded joint took place away from the weld centerline and close to the FB. For Ia of 200 A as shown in Figure 14, UTS was increased 7.4% as EN ratio was increased from 0% to 50%. However, it was found that δ first increased 27.9% when the EN ratio was increased from 0% to 30% and later it decreased 6.0% when the EN ratio was increased from 30% to 50%. The fracture of the welded joints did not occur in the middle of the weld. Instead, all samples were fractured on the weld joint sides, which was confirmed to be the weakest point in welded joints. It shows that, during the welding, an exorbitant amount of heat was required to properly melt the joint sides to get a strong weld. However, a change in behavior of welded joints under tensile load at Ia of 225 A and 250 A was noticed. According to Figure 15, the highest value of UTS, i.e., 474.10 MPa was obtained at a 30% EN ratio, whereas the highest δ, i.e., 13.40, was obtained at a 50% EN ratio. It was interesting to note that, irrespective of the EN ratio, failure of the joints took place away from the FB and weld centerline. The fracture macrographs of welded specimens, as shown in the inset of Figure 15, revealed that fractures occurred 20 mm, 21 mm and 20 mm away from the weld centerline for 0%, 30% and 50% EN ratio, respectively. It shows that proper fusion occurred across the weld joints as sufficient heat was supplied to the BM. Similarly, from Figure 16 for Ia of 250 A, the highest value of UTS, i.e., 477.77 MPa, was obtained at a 0% EN ratio, whereas the highest δ, i.e., 12.78, was obtained at a 50% EN ratio. The fracture for all of the samples occurred away from the FB and weld centerline. Fractures occurred 22 mm, 21mm and 21mm away from the weld centerline for 0%, 30% and 50% EN ratio, respectively. It was found that the welds made by using high currents offer very good strength and elongation.

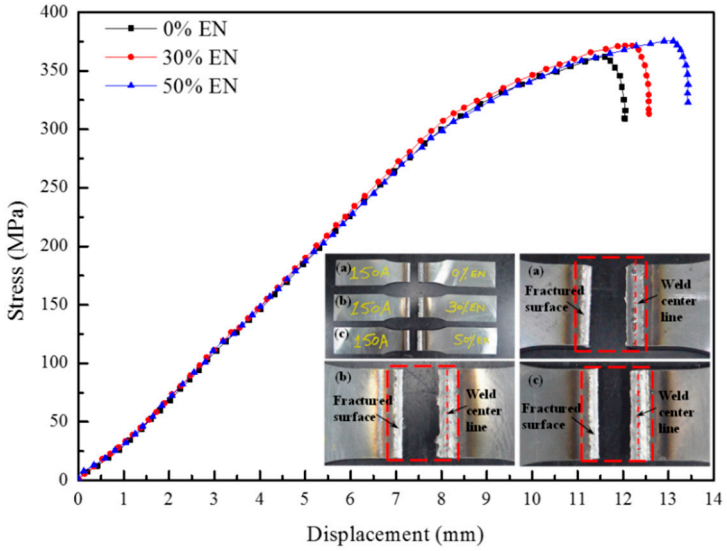

Figure 12. Stress vs. displacement at Ia of 150 A. The inset shows the fractured surfaces of the tested samples.

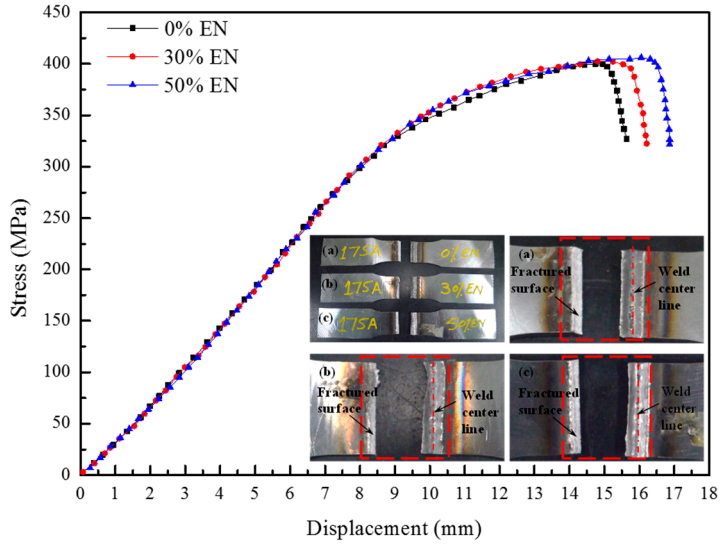

Figure 13. Stress vs. displacement at Ia of 175 A. The inset shows the fractured surfaces of the tested samples.

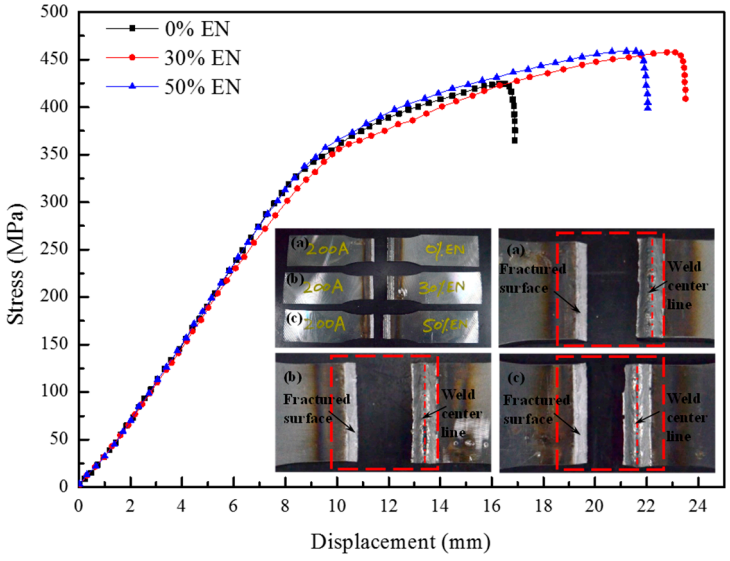

Figure 14. Stress vs. displacement at Ia of 200 A. The inset shows the fractured surfaces of the tested samples.

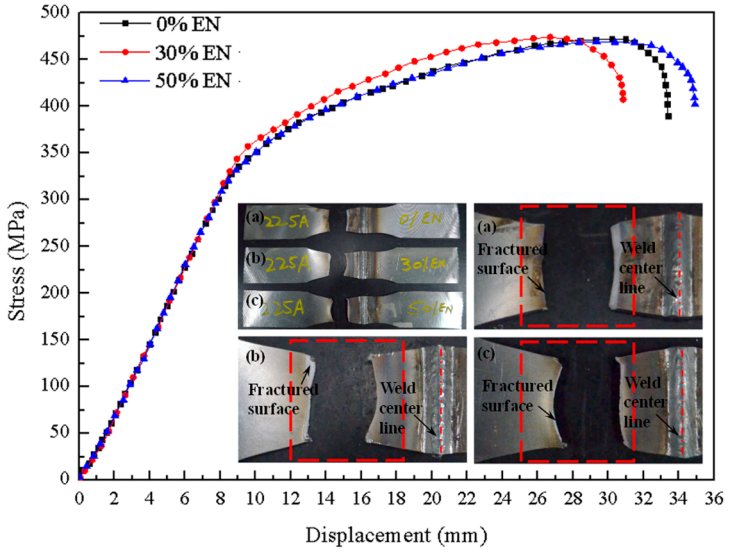

Figure 15. Stress vs. displacement at Ia of 225 A. The inset shows the fractured surfaces of the tested samples.

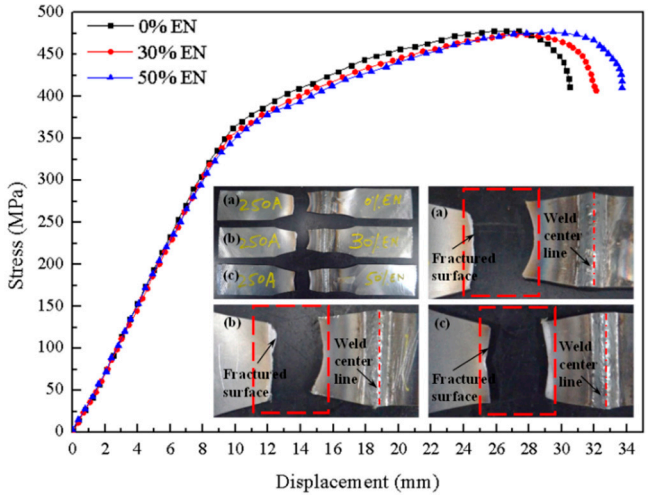

Figure 16. Stress vs. displacement at Ia of 225 A. The inset shows the fractured surfaces of the tested samples.

Table 3. Tensile tests results of welded joints.

Sr. No.	Weld Description	Ultimate Tensile Strength (UTS) (MPa)	Yield Strength (YS) (MPa)	Percentage Elongation (δ) (%)
1	150 A (0%)	360.52	116.53	4.64
2	150 A (30%)	370.61	123.29	4.80
3	150 A (50%)	375.34	119.08	5.24
4	175 A (0%)	399.94	116.35	6.03
5	175 A (30%)	402.19	117.90	6.30
6	175 A (50%)	406.11	110.76	6.57
7	200 A (0%)	424.45	134.00	6.66
8	200 A (30%)	457.71	124.16	9.24
9	200 A (50%)	458.80	98.19	8.71
10	225 A (0%)	472.01	318.67	13.2
11	225 A (30%)	474.10	320.13	11.65
12.	225 A (50%)	469.27	324.64	13.4
13	250 A (0%)	477.77	322.85	11.66
14	250 A (30%)	473.45	322.12	12.18
15	250 A (50%)	476.92	324.64	12.78

3.4. Micro-Section Analysis and Micro-Hardness Testing

In the final part of the present work, micro-hardness testing and micro-section analysis were performed. For the welding joint test, a Micro Vickers hardness tester (Mitutoyo, Aurora, IL, USA) was used to measure the hardness of the welded samples. A Vickers hardness test with a load of 1.961 N was used to measure the hardness. The selected welded samples were experimented at Ia of 250 A and three EN ratios. Measurements were conducted on BM, fusion zone (FZ) and HAZ. Figure 17 shows the hardness distribution measured at a distance of 2 mm below the top of the base plate. It was found that at the same value of current, i.e., 250 A but at different EN ratios, the micro-hardness distribution was not strikingly affected. The measured average hardness of the BM was found to be 160 HV, whereas, in the FZ, the maximum hardness was found to be 213 HV. The higher hardness value was found in the FZ followed by low hardness in HAZ. The lower hardness in the HAZ is due to the fact that coarse grains appeared in HAZ, which resulted in the lower hardness in this zone. For understanding the microstructures of welded joints, microstructures of the welded joint at Ia of 250 A and 50% EN ratio were visualized. The microstructures of different zones of interest like weld metal, HAZ and FB were viewed. The microstructures, after polishing and macro-etching, the cross sections of the joints were captured with an optical microscope (AmScope, Irvine, CA, USA) coupled with an image analyzing software (AmScope, Irvine, CA, USA) to facilitate measuring of the details like cross-section areas of the faces and roots of weld metals as shown in Figure 18. The microstructure of the BM from Figure 18a revealed that grains were oriented in the rolling direction. The microstructure of the BM was composed of ferrite and pearlite. The microstructure of the BM was the layer laminated structure of distribution of ferrite and pearlite. The light regions were ferrite and dark ones are pearlite. The amount of pearlite was relatively small. From Figure 18b, microstructure of the welded joint in the weld metal showed columnar grains that are dendritic. Figure 18c shows the microstructure of the HAZ. The grain morphology in HAZ was different from the BM. The microstructure of the HAZ showed large grains. The increase of the grain size was due to high heat input and low cooling rates. Low cooling rate increased the size of the grains. Figure 18d shows the boundary between FZ and HAZ. Large grains were observed in HAZ near the FZ.

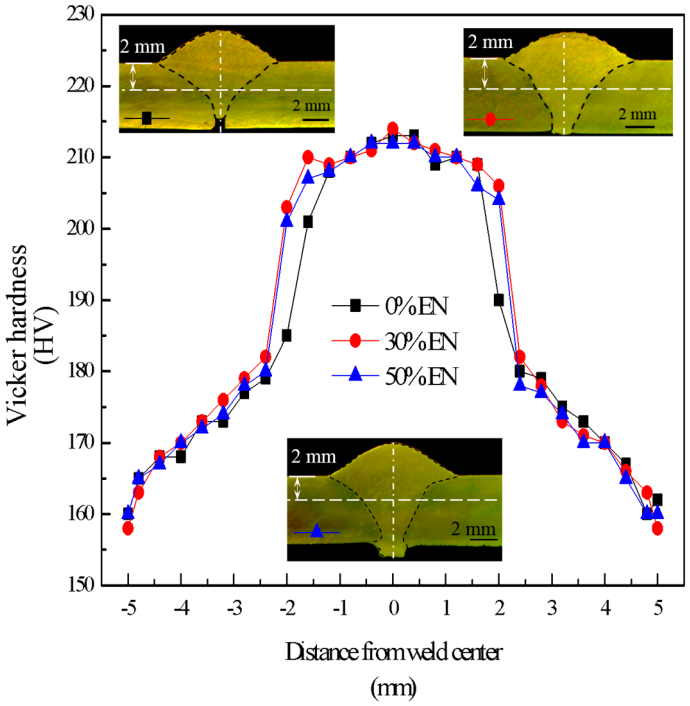

Figure 17. Vickers hardness distribution across weld joint.

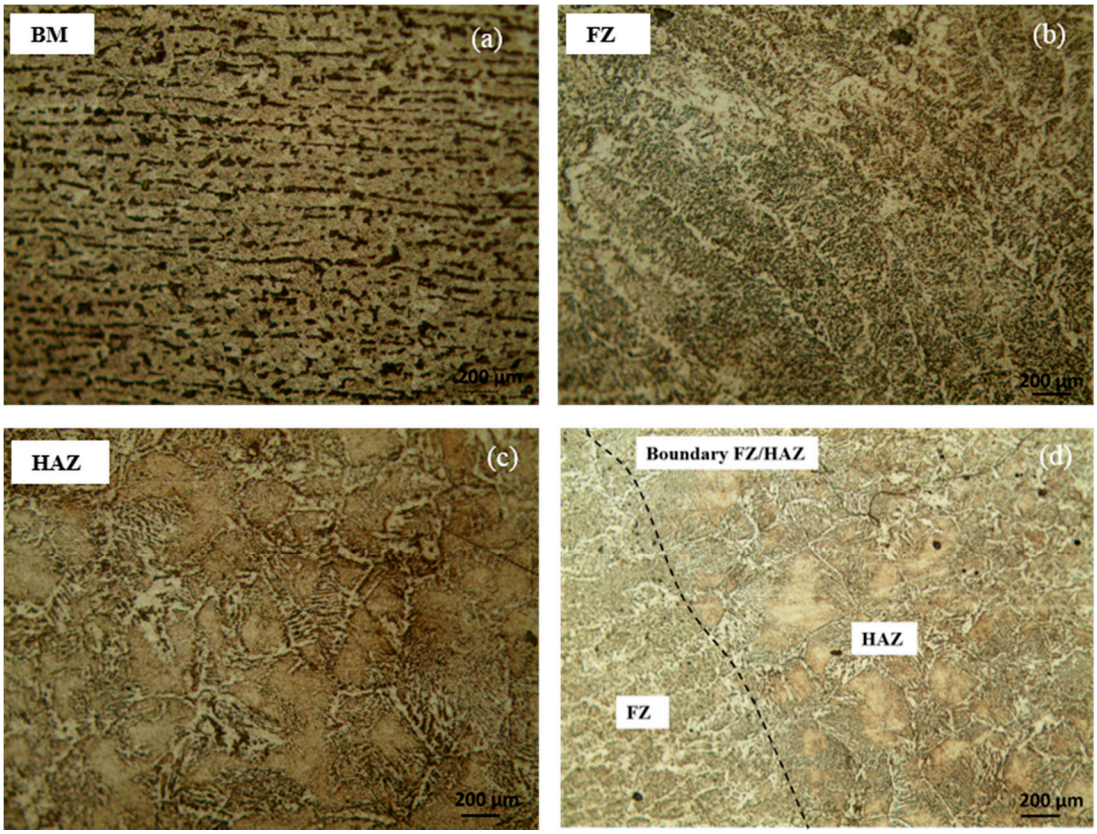

Figure 18. Microstructures (**a**) BM (base metal); (**b**) FZ (fusion zone); (**c**) HAZ (heat affected zone); and (**d**) boundary differentiating HAZ and FZ.

4. Conclusions

In the present paper, the microstructural and mechanical properties of welding joined by AC-GMAW for 5 mm thick steel plate was investigated on square groove butt joints at different settings of current and electrode negative (EN) ratios. The following conclusions were drawn:

(1) At lower values of currents, the penetration depth decreased with the increase in EN ratio. The penetration depth is less at a 50% EN ratio as compared to 0% and 30%.
(2) At higher values of currents, an increase in EN ratio resulted in an increase in penetration depth. At high currents of 225 A and 250 A with 50% EN ratios, the highest penetration was found. Moreover, it was concluded that by changing the EN ratio, the depth of penetration can be controlled.
(3) The mechanical properties were greatly influenced by the current and EN ratio settings. The tensile strength improved with increasing current, whereas the percentage elongation increased with increasing EN ratio. The maximum UTS, i.e., 477.77, was achieved at welding current of 250 A and 0% EN ratio, whereas high percentage elongation was obtained at 225 A and a 50% EN ratio.
(4) Under the settings of 250 A and varying EN ratios, micro-hardness distribution was not strikingly affected. Moreover, low hardness values were found in the HAZ as compared to the FZ.
(5) The AC-GMAW process at high currents and EN ratios can be a solution to join thick steel plates with a minimum number of passes. It is recommended that, under the current settings of 250 A and 50% EN ratios, sound welds can be obtained for thick plates.
(6) A detailed study for understanding the gap bridging capability of the AC-GMAW process at different joint gaps, welding speed and thickness of plates are required to analyze optimal filling of molten metal in the joint gap and the effect of these parameters on mechanical properties.

Acknowledgments: This research was supported by the Ministry of Trade, Industry & Energy (MOTIE, Korea) under Industrial Technology Innovation Program No. 10067156, 'Development of heavy structure dimensional accuracy measurement and management software system for improving productivity in shipbuilding company', and No. 10050495, 'Development of simulation based production management systems for middle-sized shipbuilding companies'.

Author Contributions: Adeel Ikram conceived the research. He designed and performed the experiments and analyzed the data. Hyun Chung academically supervised the research. Both authors contributed to the manuscript preparation and have given approval to the final version of the manuscript.

Conflicts of Interest: The authors declare no conflict of interest.

References

1. Tong, H.; Ueyama, T.; Harada, S.; Ushio, M. Quality and productivity improvement in aluminium alloy thin sheet welding using alternating current pulsed metal inert gas welding system. *Sci. Technol. Weld. Join.* **2001**, *6*, 203–208.
2. Ikram, A.; Arif, N.; Chung, H. Design of an induction system for induction assisted alternating current gas metal arc welding. *J. Mater. Process. Technol*. **2016**, *231*, 162–170.
3. Huismann, G. Determining cooling time t8/5 on AC-GMAW in comparison to DC-pulse welding. In Proceedings of the International Symposium on Visualization in Joining & Welding Science through Advanced Measurements and Simulation, Osaka, Japan, 17–18 October 2016; Volume 1, pp. 45–46.
4. Harwig, D.D.; Dierksheide, J.E.; Yapp, D.; Blackman, S. Arc behavior and melting rate in the VP-GMAW process. *Weld. J*. **2006**, *85*, 52–62.
5. Kim, T.J.; Lee, J.P.; Min, B.D.; Yoo, D.W.; Kim, C.U. Characteristics of pulse MIG arc welding with a wire melting rate change by current polarity effect. *J. Electr. Eng. Technol.* **2007**, *2*, 366–372.
6. Talkington, J.E. Variable Polarity Gas Metal Arc Welding. Master's Thesis, Department of material science and engineering, Ohio State University, Columbus, OH, USA, 1998.
7. Park, H.J.; Kim, D.C.; Kang, M.J.; Rhee, S. The arc phenomenon by the characteristic of EN ratio in AC pulse GMAW. *Int. J. Adv. Manuf. Technol*. **2013**, *66*, 867–875.
8. Kumar, R.; Dilthey, U.; Dwivedi, D.K.; Ghosh, P.K. Thin sheet welding of Al 6082 alloy by AC pulse-GMA and AC wave pulse-GMA welding. *Mater. Des.* **2009**, *30*, 306–313.
9. Vilarinho, L.O.; Nascimento, A.S.; Fernandes, D.B.; Mota, C.A.M. Methodology for parameter calculation of VP-GMAW. *Weld J*. **2009**, *88*, 92s–98s.
10. Nascimento, A.S.; Fernandes, D.B.; Mota, C.A.; Vilarinho, L.O. Methodology for determination of parameters for welding MIG with variable polarity. *Weld. Int.* **2009**, *23*, 473–480.
11. Monteiro, L.S.; Scotti. A. A methodology for parameterization of the MIG/MAGCA and its application in service repair of pipelines of oil and gas. In Proceedings of the 22nd International Congress of Mechanical Engineering, Ribeirão Preto, SP, Brazil, 3–7 November 2003; pp. 8103–8117.
12. Arif, N.; Chung. H. Alternating current-gas metal arc welding for application to thin sheets. *J. Mater. Process. Technol*. **2014**, *214*, 1828–1837.
13. Kim, K.; Chung, H. Wire melting rate of alternating current gas metal arc welding. *Int. J. Adv. Manuf. Technol*. **2016**, doi:10.1007/s00170-016-9384-8.
14. Kiran, D.V.; Cheon, J.; Arif, N.; Chung, H.; Na, S.J. Three-dimensional finite element modeling of pulsed AC gas metal arc welding process. *Int. J. Adv. Manuf. Technol*. **2016**, *86*, 1453–1474.
15. Arif, N.; Chung. H. Alternating current-gas metal arc welding for application to thick plates. *J. Mater. Process. Technol*. **2015**, *222*, 75–83.
16. OTC Daihen Inc. Available online: http://www.daihen-usa.com (accessed on 3 January 2017).